https://doi.org/10.5194/egusphere-2024-1840
Preprint. Discussion started: 5 August 2024

A-year Continuous Observations of Near-Surface Atmospheric Water Vapor Stable Isotopes at Matara, Sri Lanka

Yuqing Wu [1, 2], Jing Gao [1, 3, *], Aibin Zhao [1], Xiaowei Niu [1], Yigang Liu [1, 2], Disna Ratnasekera [4, 5], Tilak Priyadarshana Gamage [6], Amarasinghe Hewage Ruwan Samantha [6]

1 State Key Laboratory of Tibetan Plateau Earth System, Resources and Environment, Institute of Tibetan Plateau Research, Chinese Academy of Sciences, Beijing 100101, China

2 University of Chinese Academy of Sciences, Beijing, 100049, China

3 Lanzhou University, Lanzhou 733000, China

4 China-Sri Lanka Joint Center for Education & Research, Guangzhou 510301, China

5 Department of Agricultural Biology, Faculty of Agriculture, University of Ruhuna, Matara 81000, Sri Lanka

6 Faculty of Fisheries and Marine Sciences & Technology, University of Ruhuna, Matara 81000, Sri Lanka

* *Corresponding to*: Jing Gao (gaojing@itpcas.ac.cn)

Abstract:

Atmospheric water vapor stable isotopes are crucial for understanding hydrological cycle processes under climate change. This study presents a year-long in-situ monitoring of atmospheric water vapor stable isotopes ($\delta^{18}O$, δD) at Matara, Sri Lanka, from March 2020 to February 2021 to assess how oceanic sources and moisture transport influence coastal atmospheric moisture isotopic composition. We identified clear seasonal patterns in the isotopic composition, with $\delta^{18}O$, δD, and d-excess showing substantial variation between the southwest and northeast monsoon periods. The primary moisture sources were the Arabian Sea and the Indian Ocean during the southwest monsoon (May to September), characterized by depleted $\delta^{18}O$ from -20.4‰ to -9.1‰. During the northeast monsoon dominated period, the northern Bay of Bengal, the Indian subcontinent, and Southeast Asia were primary moisture sources, displayed enriched δ^{18}O (-23.9‰ to -7.5‰) and higher d-excess values (up to 25 ‰). The study also identified significant influences of sea surface temperature and sea surface relative humidity, on the isotopic composition of water vapor. Additionally, outgoing longwave radiation (OLR) is a significant index used to gauge the intensity of convective activity. Lower OLR values, indicative of stronger and deeper convection, were associated with more depleted δ^{18}O in air masses. These findings help to improve the understanding of influences of the monsoon and local meteorological condition on water vapor isotopes in tropical region and provide new dataset on enhancing water vapor isotopic modeling or atmospheric processes projection in coastal regions.

Keywords: Indian Summer Monsoon, Water Vapor Isotopes, Sea Surface Condition, Convective Activity, Sri Lanka

Short Summary

This study monitored atmospheric water vapor isotopes for a year at Matara, Sri Lanka. It found clear seasonal variations in δ^{18}O, δD, and d-excess. There showed depleted δ^{18}O during the southwest monsoon, while had enriched δ^{18}O and higher d-excess during the northeast monsoon. Sea surface condition and regional convective activity significantly influenced the isotopic compositions, improving understanding of monsoon and local meteorological condition impacts on tropical water vapor.

1 Introduction

The Indian Summer Monsoon (ISM), occurring from June to September, is a pivotal component of the Asian climate system, serving as the primary transport of moisture from the Indian Ocean to the Indian subcontinent and the Tibetan Plateau (TP). Monsoonal precipitation plays a crucial role in agriculture and water resources, affecting the welfare of over 1.9 billion people in surrounding countries (Webster et al., 1998; Goswami et al., 2016). The Tibetan climate and hydrology are profoundly influenced by the ISM, as it contributes significantly to the regional water cycle by delivering substantial rainfall during the summer months. This rainfall is essential for maintaining the glaciers and permafrost in the TP, which are key sources of water for many of Asia's largest rivers (Bookhagen and Burbank, 2010). The ISM's intensity and variability can lead to significant fluctuations in water availability, affecting both agriculture and hydropower generation in the region (Singh and Bengtsson, 2004; Gao et al., 2014). Furthermore, the interaction between the ISM and the TP's topography creates unique climatic conditions that influence weather patterns and extreme events in the region (Liu and Chen, 2000).

The seasonal precipitation and its origins over the TP are inextricably linked to the dynamics of the ISM (Dai et al., 2021). Previous studies have provided evidence that isotopic records derived from precipitation over the TP offer insights into the climatic fluctuations and distinct moisture attributes associated with the ISM (Gao et al., 2013; Guo et al., 2017). The summer monsoon brings significant moisture from the Indian Ocean, leading to substantial rainfall over the TP primarily during the monsoon months during June-September (Yao et al., 2012). This seasonal influx of moisture is critical for maintaining the regional hydrological balance and supporting the ecosystems. Furthermore, the ISM's intensity and variability significantly influence the interannual and decadal precipitation patterns over the TP, affecting the overall water availability and climatic stability of the region (Kaushal et al., 2018).

The stable isotopic composition of river water (Bershaw et al., 2012; Li and Garzione, 2017), precipitation (Rahul et al., 2016a; Cai et al., 2017), and water vapor (Risi et al., 2008; Steen-Larsen et al., 2013b; Rahul et al., 2016b; Lekshmy et al., 2022) serves as a valuable tool for understanding the origins and transmission processes of atmospheric water vapor. Recent studies have significantly enhanced our understanding of isotopic signals in convection regions, illuminating the complex interactions between moist processes and isotopic compositions in tropical deep convection. In the winter trades near Barbados, vertical transport and large-scale circulations have been identified as primary drivers of isotopic variability at the cloud base, acting over timescales from hours to days (Bailey et al., 2023; Villiger and Aemisegger, 2024). Investigations into water vapor isotopes in the West African troposphere reveal that both convection and mixing emphasize the important role of large-scale atmospheric circulation processes in the variations of water vapor isotopes (Diekmann et al., 2021; de Vries et al., 2022). The mechanisms by which convective activity lowers stable isotope values of water vapor and precipitation are still under debate. Some researchers emphasize the significance of condensation levels (Cai and Tian, 2016; Permana et al., 2016; Thompson et al., 2017), while others point to raindrop re-evaporation and raindrop-vapor isotope exchange during strong convection as crucial factors (Galewsky et al., 2016). Additionally, unsaturated or mesoscale descending airflows that transport vapor depleted in heavy isotopes to the lower atmosphere also contribute to lower isotope values (Risi et al., 2008; Kurita, 2013). The influence of these processes varies with the intensity of convective activity. These studies provide valuable insights. However, there is a paucity of study on the Indian Ocean, particularly in relation to Sri Lanka. This gap underscores the need to explore isotopic signals in this region, with reference to established findings by Risi et al. (2008) and other seminal works. Comparison with the above results, recent studies on water stable isotopes in the South Indian Ocean and South Asian region have uncovered connections between local processes and atmospheric circulation, shedding light on sea-surface dynamics (Midhun et al., 2013; Rahul et al., 2016b; Bonne et al., 2019). Fractionation occurs during various phase transitions, such as sea surface evaporation, condensation beneath clouds, re-evaporation of raindrops, and diffusive exchange between water vapor and raindrops (Stewart, 1975; Benetti et al., 2018; Graf et al., 2019). The occurrence of fractionation unveils investigable spatiotemporal distribution patterns in the water isotopic composition, encompassing water vapor and precipitation. Deuterium excess (d-excess = $\delta D - 8 \times \delta^{18}O$) is a useful parameter for studying kinetic fractionation effects (Dansgaard, 1964). Compared to other water stable isotopes, such as those found in precipitation and surface water, the monitoring of atmospheric water vapor isotopes is not limited by season, weather, or location (Angert et al., 2008). This capability for full-time and full-space observation allows for the avoidance of information loss during

https://doi.org/10.5194/egusphere-2024-1840
Preprint. Discussion started: 5 August 2024

sampling, thereby providing a more comprehensive, continuous insight into the evolving processes of atmospheric water vapor transport from diverse sources and a thorough understanding of isotope transformation processes within the water cycle.

Evaporation at the ocean surface constitutes a significant component of the global water cycle and is pivotal in accurately modeling climate change. The primary objective of research on water vapor stable isotopes in the marine boundary layer aims to elucidate the processes and influencing factors of evaporation isotopes (Craig and Gordon, 1965). The d-excess of evaporated water vapor is predominantly impacted by dynamic fractionation associated with sea surface temperature (SST), the relative humidity of the sea-surface air (RH_{SST}, calculated relative to the saturation vapor pressure at SST), and wind speed (rough or smooth) (Benetti et al., 2015; Benetti et al., 2018). Investigations into the water vapor stable isotopic composition within the marine boundary layer have been principally concentrated around regions including a large part of the North Atlantic Ocean (such as Greenland, Iceland, Bermuda) (Steen-Larsen et al., 2013a; Bonne et al., 2014; Benetti et al., 2018; Bonne et al., 2019), Bay of Bengal (BoB) (Lekshmy et al., 2022), and the ocean throughout the Atlantic and Arctic Oceans (Kurita, 2011). These studies have validated the negative relationship between d-excess and RH_{SST} (Uemura et al., 2008; Steen-Larsen et al., 2015), suggesting that wind speed and SST exert limited influence on this correlation (Benetti et al., 2015). Observations from the North Atlantic bolster this theory (Benetti et al., 2014). In addition, it also highlights the significant variations in d-excess values from different moisture sources (Kurita, 2011; Steen-Larsen et al., 2013b; Delattre et al., 2015). Subsequently, Benetti et al. (2015) introduced a multi-layer mixing model, which is expected to advance the accuracy of d-excess and water vapor isotope simulations. Due to the impact of dynamic fractionation on sea surface evaporation, some studies have focused on simulating observed d-excess under the closure assumption (Bonne et al., 2019). Furthermore, researchers have used isotope atmospheric circulation models to assess mixing and transport processes within the marine boundary layer (Benetti et al., 2015). Owing to the minor influence of transport-induced fractionation, d-excess of the marine boundary layer is conventionally employed to deduce moisture sources (Benetti et al., 2018).

Amidst the current backdrop of global climate change, observing stable isotopes in atmospheric water vapor is vital for monitoring and comprehending climate shifts in tropical low-latitude areas (Rahul et al., 2016b). Such research is instrumental in providing a deeper understanding of near-surface water vapor dynamics, pinpointing vapor sources and transport routes, and differentiating the contributions of atmospheric water vapor to the water cycle. Positioned in the northern expanse of the Indian Ocean, Sri Lanka experiences pronounced impacts from both the southwest monsoon and the northeast monsoon (Fig. 1a, b). It emerges as a prominent origin region for monsoonal water vapor in the TP. Therefore, investigating the dynamics and variations of near-surface atmospheric water vapor stable isotopes at coastal stations, pivotal for monitoring monsoonal water vapor source regions, enhances our understanding of precipitation processes in the Indian Ocean. Oceanic evaporation serves as the inaugural stage in the global water cycle phase transition. The primary objective of researching water vapor stable isotopes is to comprehend the processes and controlling factors of water isotopic variations.

In this study, we conducted continuous observations of near-surface atmospheric water vapor stable isotopes in Matara, Sri Lanka, from March 1, 2020, to February 28, 2021. Our goal is to understand the main variations in moisture sources and transmission processes in tropical coastal regions, and to explore how sea surface processes, convective activity, and local meteorological factors affect near-surface atmospheric water vapor stable isotopes at a coastal station, across daily, monthly, and seasonal (monsoonal) time scales. Section 2 gives an overview of the study site, covering meteorological and water vapor observations, calibration protocols, and analysis methods. In Section 3, we illustrate the variability of isotopic and meteorological parameters, analyze moisture sources, assess the impact of sea surface processes on water vapor isotopes, and explore the relationship between water vapor isotopes, convective activity, and local meteorological observations.

2 Data and methods

2.1 Study site and meteorological data

Sri Lanka (between 6°N to 10°N and 79° to 82°E), the southernmost country of the Indian subcontinent, is a key region for identifying the moisture source of the south Asian summer monsoon (Ravisankar et al., 2015). Features a tropical climate, Sri Lanka experiences four distinct monsoon seasons annually: the northeast monsoon from December to February, the first inter-monsoon from March to April, the southwest monsoon from May to September, and the second inter-monsoon from October to November (Malmgren et al., 2003; Jayasena et al., 2008). Most of the precipitation in Sri Lanka comes from the southwest and northeast monsoon systems, accounting for over 70% of the total annual precipitation (Fig. 1c). Precipitation formation in Sri Lanka primarily relies on organized convection associated with the Intertropical Convergence Zone (ITCZ) and low-pressure systems (Gadgil, 2003), and the moisture that derives precipitation is primarily derived from the Indian Ocean and BoB (Bandara et al., 2022). The southwest monsoon transports moisture from the Indian Ocean to southwestern Sri Lanka (Fig. 1a, b), leading to increased rainfall in the southwestern region of Sri Lanka compared to the northeast (Bavadekar and Mooley, 1981). Similarly, the northeast monsoon carries water vapor from the BoB to the north and northeast of Sri Lanka, where it produces disproportionately high amounts of rainfall compared to the southwest of the country (Dhar and Rakhecha, 1983; Wang, 2006).

An automated weather station (AWS) was installed at the University of Ruhuna, Matara (located at 5.94°N, 80.57°E) on the southern coast of Sri Lanka. It collected real-time meteorological observations, including air temperature, precipitation, relative humidity, vapor pressure, wind speed, and wind direction, from March 1, 2020, to February 28, 2021. Meteorological data are compared with water vapor isotopic data measured during the same period. The annual average precipitation is 2085 mm, and the annual average air temperature is 27.58°C based on the European Centre for Medium-Range Weather Forecasts (ECMWF, https://cds.climate.copernicus.eu/eu/) reanalysis dataset (ERA5) from 2000 to 2020 (Fig. 1c) (Hersbach et al., 2020).

https://doi.org/10.5194/egusphere-2024-1840
Preprint. Discussion started: 5 August 2024

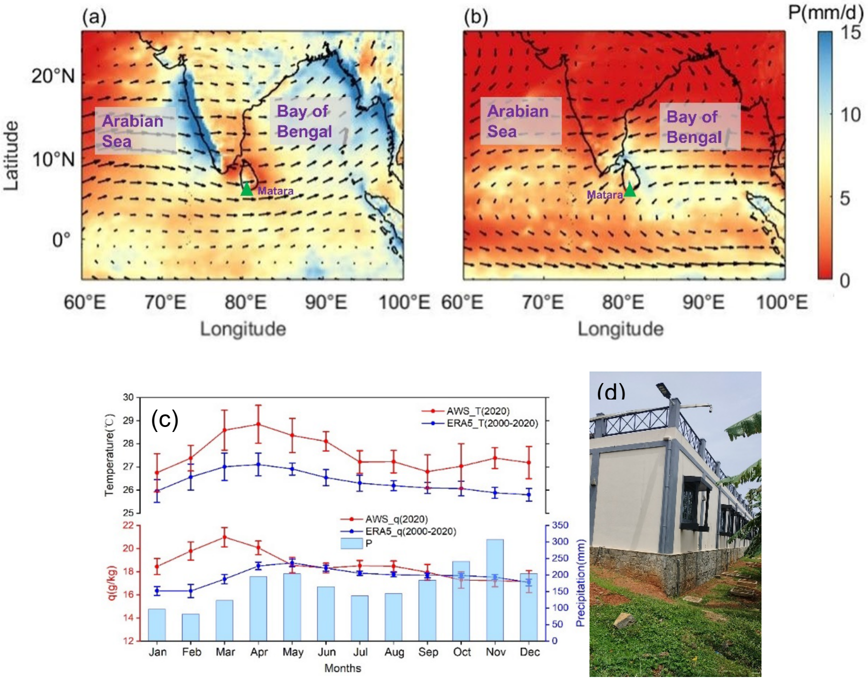

Figure 1: Mean Wind Vectors (Arrows) at 850 hPa during the (a) 2020 Southwest Monsoon and (b) 2020/2021 Northeast Monsoon Seasons, along with Mean Precipitation (P, light blue rectangle) for the same. (c) Monthly Temperature and Specific Humidity (q) obtained from an automated weather station at Matara station (averaged for the years 2020-2021), as well as Monthly Average Temperature, Specific Humidity, and Precipitation (from ERA5, averaged for the years 2000-2020). (d) Photograph of the top floor platform at the University of Ruhuna where the system is installed.

In this study, we used daily and monthly averages of outgoing longwave radiation (OLR, https://www.esrl.noaa.gov/psd/data/gridded/data.ncep.reanalysis.pressure.html) to quantify the convective activity. In addition, we used hourly data of 2m air temperature, 2m dew temperature, air pressure, precipitation, evaporation, SST, atmospheric boundary layer height (BLH), wind speed, and wind direction obtained from ERA5 for years 2000 to 2021, with a spatial resolution of 0.25°×0.25° and a temporal resolution of hourly. Studies have shown that ERA5 temperature, precipitation and other data provide good representations of the Matara equatorial climate and can

https://doi.org/10.5194/egusphere-2024-1840
Preprint. Discussion started: 5 August 2024

be used in lieu of missing observational data (Bandara et al., 2022). For the atmosphere above open sea regions, RH_{SST} is obtained by the following formula (Bonne et al., 2019):

$$RH_{SST} = RH_{2m\ air} \times \frac{q_{sat}(T_{2m\ air})}{q_{sat}(SST)} \quad (1)$$

where $RH_{2m\ air}$ is the relative humidity at 2m above the ocean surface, $q_{sat}(T_{2m\ air})$ is the specific humidity at a saturated condition for a given 2m air temperature, and $q_{sat}(SST)$ is calculated for seawater at salinity of 35 Practical salinity units (PSU) (Curry and Webster, 1999).

The calculation formulas for air saturation specific humidity $q_{sat}(T_{air})$ and sea surface saturation specific humidity $q_{sat}(SST)$ are:

$$q_{sat}(T_{air}) = \frac{0.622 \times E}{P} \quad (2)$$

$$q_{sat}(SST) = 0.98 \times q_s(\text{sea surface salinity of 35 PSU}) \quad (3)$$

among them, the calculation method of q_s(sea surface salinity of 35 PSU) is the same as that of $q_{sat}(T_{air})$. E is the saturated water vapor pressure, obtained from the improved Goff-Gratch formula (Goff and Gratch, 1946). P is atmospheric pressure, and the sea surface pressure is taken as a fixed value of 1013.25 hPa for calculation.

2.2 In-situ Observation of Atmospheric Water Vapor Isotopic Compositions

At the Matara site, near-surface atmospheric water vapor isotope measurements aim to establish a continuous, high-resolution dataset with one-second time intervals. This study utilizes a Water Vapor Isotope Analyzer (manufactured by Los Gatos Research (LGR) Inc.) in conjunction an LGR Water Vapor Isotope Standard Source (WVISS model). The LGR instrument leverages Off-Axis Integrated Cavity Output Spectroscopy (Off-Axis ICOS), a laser spectroscopic technique. This method integrates a laser resonance cavity with a gas measurement chamber, where the laser oscillates repeatedly between mirrors at the ends of the cavity. Only a small fraction of the laser reaches the detector after traversing the sample gas thousands of times, effectively increasing the chamber's thickness and significantly enhancing the water vapor absorption signal. This allows for the detection of low concentrations of D and ^{18}O in water vapor (Liu et al., 2015). Compared to traditional methods, this spectroscopic technique offers three advantages: it is compact and portable, enabling real-time field monitoring; it can simultaneously measure δ^{18}O and δD; and it has lower measurement costs and requires less operator expertise, facilitating broader adoption.

The analytical system for measuring atmospheric water vapor stable isotopes in Sri Lanka situated approximately 100 meters from the sea (5.94° N, 80.57° E, 10 meters), consists of four primary components: (1) Sampling inlet it positioned approximately 5 meters above the ground, atop the office building of the China Sri Lanka Joint Center for Education and Research at the University of Ruhuna (see Figure 1d). The inlet is equipped with a stainless-steel mesh to prevent the interference of insects and directed downward to avoid direct rain splashes. (2) A 1/4-inch outer diameter stainless steel tubing was used. The sampling tube is insulated with heating tape and 2-cm thick insulation pipe to maintain warmth. (3) XX generates a constant water vapor flow with known isotopic composition at different humidity levels. (4) Water vapor isotope analyzer. In this study, the measurement precision of δ^{18}O and δD reaches 0.25‰ and 0.5‰, respectively, at a concentration of 2500 ppmv. This setup minimizes external influences and maintains the integrity of the sampled water vapor.

The water vapor analytical system is located adjacent to the AWS, ensuring a high level of synchrony between the water vapor stable isotope data and meteorological measurements. We define wind directions ranging from 60° to 330°N are defined as reflecting the ocean region, while those from 330° to 60°N reflect the land (Figure 1).

The δ notation, expressed in per mil (‰), is used to represent the atmospheric water vapor stable isotopes, using the following equations:

$$R_{^{18}O} = \frac{{}^{1}H_2{}^{18}O}{{}^{1}H_2{}^{16}O} \quad (4)$$

$$R_D = \frac{{}^{1}H\,{}^{2}H\,{}^{16}O}{{}^{1}H_2\,{}^{16}O} \tag{5}$$

$$\delta_{sample} = \left(\frac{R_{sample}}{R_{VSMOW}} - 1\right) \times 1000‰ \tag{6}$$

Here, δ_{sample} represents either $\delta^{18}O$ or δD, indicating the ^{18}O or D isotope ratio relative to Vienna Standard Mean Ocean Water (VSMOW) in the sample. R_{sample} and R_{VSMOW} are the ^{18}O or D sample and VSMOW isotope ratios.

2.3 Calibration Protocol

In this study, we adhere to the calibration protocol proposed by Steen-Larsen et al. (2013b). Briefly, the instrument calibration and data processing consist of three major steps: (1) instrumental humidity-isotope response calibration, (2) Vienna Standard Mean Ocean Water - Standard Light Antarctic Precipitation (VSMOW-SLAP) calibration, and (3) drift correction (refer to Text 1 in the Supporting Information).

The water vapor concentration can influence the measured water vapor isotopic composition, known as concentration- or humidity-isotope dependency characterization. By introducing a constant stream of water vapor concentration with a known isotopic composition at different humidity levels, we can establish the humidity-isotope response function (Sturm and Knohl, 2010; Aemisegger et al., 2012). As this function may vary over time, the humidity-isotope response calibration was repeated monthly, using two standard samples with well-known isotopic compositions measured at humidity levels ranging from 16,000 to 38,000 ppmv at intervals of 1000 ppmv, to establish a correction function. Each measurement level was conducted for a minimum of 25 minutes using the LGR WVISS. Our results are referenced to a humidity level of 20,000 ppmv. We compared our measurements to the international VSMOW-SLAP scale, assuming a linear drift between calibration points.

All measurements are subject to instrumental internal drift, necessitating correction through a specific drift-correction procedure. To compensate for this drift, the LGR WVISS generates water vapor from a drift-standard bottle is measured for 25 minutes after each 12 hours of ambient air measurements. Furthermore, this drift-standard water is sampled at each routine maintenance interval. Laboratory analyses of liquid isotopes have confirmed the stability of its isotopic composition over time. A linear drift is assumed between each drift-standard measurement.

2.4 Rayleigh Distillation Model and MBL-Mix Model

The Rayleigh distillation model is employed to quantify isotopic variations during phase changes (Dansgaard, 1964), wherein the residual air mass becomes drier with a depletion in heavy isotopes following moist adiabatic vertical ascent (Gat, 1996):

$$R_r = R_0 f^{\alpha_v^l(T) - 1} \tag{8}$$

Here, R_r and R_0 represent the isotopic ratio of residual vapor and initial vapor, respectively. $\alpha_v^l(T)$ denotes the equilibrium fractionation factor, and f is the fraction of residual water vapor.

By integrating the definition of isotope ratios as given in Equation (6), the Rayleigh distillation model formula can be expressed in terms of isotopic content as follows:

$$\delta_r = (\delta_0 + 1) f^{\alpha_v^l(T) - 1} - 1 \tag{9}$$

Where δ_r and δ_0 are the isotope ratios relative to Vienna Standard Mean Ocean Water (VSMOW) in the sample of residual vapor and initial vapor, respectively.

Meanwhile, we employ the mixing model to examine the isotopic characteristics after the mixing of two air masses (Galewsky and Hurley, 2010):

$$R_{mix} = \frac{f[HDO]_1 + (1 - f) \times [HDO]_2}{f[H_2O]_1 + (1 - f) \times [H_2O]_2} \tag{10}$$

Where R_{mix} represents the isotopic ratio of the mixed air mass, [HDO] and [H_2O] denote the isotopic water vapor volume mixing ratio, and f is the mixing fraction.

Given that Matara is a coastal city, we utilize a framework employing water vapor isotopes to study mixing processes in the marine boundary layer (MBL) (Benetti et al., 2018), utilizing the following equation:

$$1 + \delta_e = \frac{1}{\alpha_k} \times \frac{\alpha_{eq}^{vl} \times (1 + \delta_{OC}) - RH_{SST} \times \ (1 + \delta_{MBL})}{1 - RH_{SST}} \tag{11}$$

Where α_{eq}^{vl} represents the equilibrium fractionation factor between vapor and liquid, and α_k is the kinetic fractionation factor. δ_{OC} denotes the isotopic composition of the ocean surface. We utilize α_{eq}^{vl} from Majoube (1971a, b) and α_k for the smooth regime ($\alpha_k{}^{18}O = 1.006$ and $\alpha_k D = 1.0053$) (Merlivat and Jouzel, 1979).

2.5 Concentration-Weighted Trajectory and Moisture Source Diagnoses

To delineate water vapor transport paths and pinpoint moisture sources, we employed the Hybrid Single-Particle Lagrange Integrated Trajectory (HYSPLIT) model from the US National Oceanic and Atmospheric Administration (NOAA) to compute backward trajectories of air masses associated with the southwest and northeast monsoons. The Global Data Assimilation System (GDAS) with 1°×1° and 3-hour spatial and temporal resolutions furnished the background meteorological data from May 2020 to September 2020 and December 2020 to February 2021 (ftp://arlftp.arlhq.noaa.gov/archives/gdas1/). As atmospheric water vapor primarily resides at altitudes below 2 km (Wallace and Hobbs, 2006), we initiated the backward trajectories from a height of 50 m above the ground. Additionally, we computed 7-day backward trajectories at 00:00h, 06:00h, 12:00h, and 18:00h during each monsoon period and utilized K-means clustering to calculate specific humidity along each trajectory.

Based on the HYSPLIT outcomes, we derived the concentration-weighted trajectory (CWT) field at a resolution of 0.5°×0.5° (Hsu et al., 2003) using the in-situ daily average $\delta^{18}O$ and d-excess in water vapor along each backward trajectory. This facilitated the identification of potential moisture sources and assessment of recirculation's influence on d-excess in water vapor (Salamalikis et al., 2015; Bedaso and Wu, 2020; Xu et al., 2022). CWT (C_{ij}) was calculated as:

$$C_{ij} = \frac{\sum_{k=1}^{K} C_k \tau_{ijk}}{\sum_{k=1}^{K} \tau_{ijk}} \qquad (12)$$

Where (i, j) denote grid coordinates, k represents the trajectory index, K is the total number of trajectories analyzed, C_K is the concentration (here $\delta^{18}O$ and d-excess) measured upon trajectory k's arrival, and τ_{ijk} is the residence time of trajectory k in grid

https://doi.org/10.5194/egusphere-2024-1840
Preprint. Discussion started: 5 August 2024

cell (i, j). During this computation, the residence time is substituted by the number of trajectory endpoints in grid cell (i, j).

3 Results

3.1 Seasonal Variability of Water Vapor Stable Isotope

Figure 2 illustrates the hourly and daily averages of water vapor isotopes ($\delta^{18}O$, δD, and d-excess) alongside temperature, relative humidity, atmospheric pressure, and specific humidity from March 1, 2020, to February 28, 2021, at Matara station.

A clear seasonal cycle is evident in average values (Fig. 2 and Table 1) for relative humidity, specific humidity, lifting condensation level (LCL), monthly precipitation, and water vapor isotopic composition ($\delta^{18}O$, δD, and d-excess). Over the 12-month observation period, average temperature and relative humidity stand at 27.6°C and 80.7%, respectively (Table 1). Temperature variations maintain consistent amplitudes between monsoon and non-monsoon periods at around 10°C. Recorded minimum and maximum temperatures are 22.3°C and 21.5°C, respectively. Specifically, comparing monthly variations in air temperature and specific humidity (Fig. S3), both parameters gradually decrease from relatively high values in May, reaching a minimum in September, with monthly averages of 26.9°C and 18.5 g/kg, respectively. From January, both air temperature and specific humidity show continuous increases, peaking in May with monthly averages of 28.4°C and 21 g/kg. Mean relative humidity peaks in May at 95%, with lower values observed during winter and early spring (December to April), reaching a minimum of 49.2% in January. From late May, specific humidity gradually declines, stabilizing after mid-July and lasting until October, with levels ranging from 16 g/kg to 20 g/kg. During this period, significant oscillations of approximately 1.3 g/kg occur during the southwest monsoon, with corresponding amplitudes doubled during the northeast monsoon, at approximately 2.3 g/kg. During the southwest monsoon, temperature, and specific humidity peak in May (monthly averages of 28.4 ± 1.4°C and 21.0 ± 1.1 g/kg). February marks the coldest and driest (specific humidity) month (monthly averages of 27.4 ± 2.6°C and 17.1 ± 1.3 g/kg) during the northeast monsoon

(Fig. S3). The seasonal temperature variations exhibit modest amplitudes (Fig. 2), attributed to the tropical location of the Matara station near the equator. Conversely, relative humidity displays higher amplitude in seasonal variations compared to synoptic variations. Furthermore, daily average SST consistently exceed the daily average 2m air temperatures recorded by the AWS station (Fig. 2).

Yearly averages for water vapor isotopic values are -11.6‰ for δ^{18}O, -79.5‰ for δD, and 13.3‰ for d-excess, respectively, isotopic composition ranges from -23.9‰ to -7.5‰ for δ^{18}O, -173.2‰ to -53.4‰ for δD, and -1.2‰ to 28.1‰ for d-excess (Table 1). Monthly averages of water vapor isotopes (δ^{18}O and d-excess) exhibit stability from March to October, followed by sudden decreases. δ^{18}O and δD show distinct seasonal variations, with higher values during the southwest monsoon period and lower values during the northeast monsoon period (Table 1). δ^{18}O decreases through the southwest monsoon, non-monsoon, and northeast monsoon periods, with mean values of -11.1‰, -11.9‰, and -12.2‰, respectively. Extreme values of δ^{18}O are observed during the northeast monsoon, with a maximum of -7.5‰ and a minimum of -23.9‰. Conversely, d-excess follows a reverse pattern to δ^{18}O on both seasonal and monthly scales, characterized by lower values during the southwest monsoon and higher values during the non-monsoon period. d-excess increases sequentially through the northeast monsoon, southwest monsoon, and non-monsoon periods, with mean values of 12.4‰, 13‰, and 14.7‰, respectively. The d-excess maximum occurs in November at 28.1‰ (monthly average of 15.2 ± 4.3‰), while the minimum of -1.2‰ is recorded in January (monthly average of 11.3 ± 4.5‰). The d-excess peaks in April 2020 at 19.1‰, indicating potential contributions from local recycling. Low specific humidity corresponds to depleted δ^{18}O and elevated d-excess values, indicating strong depletion during long-distance transport from source regions to the observation station.

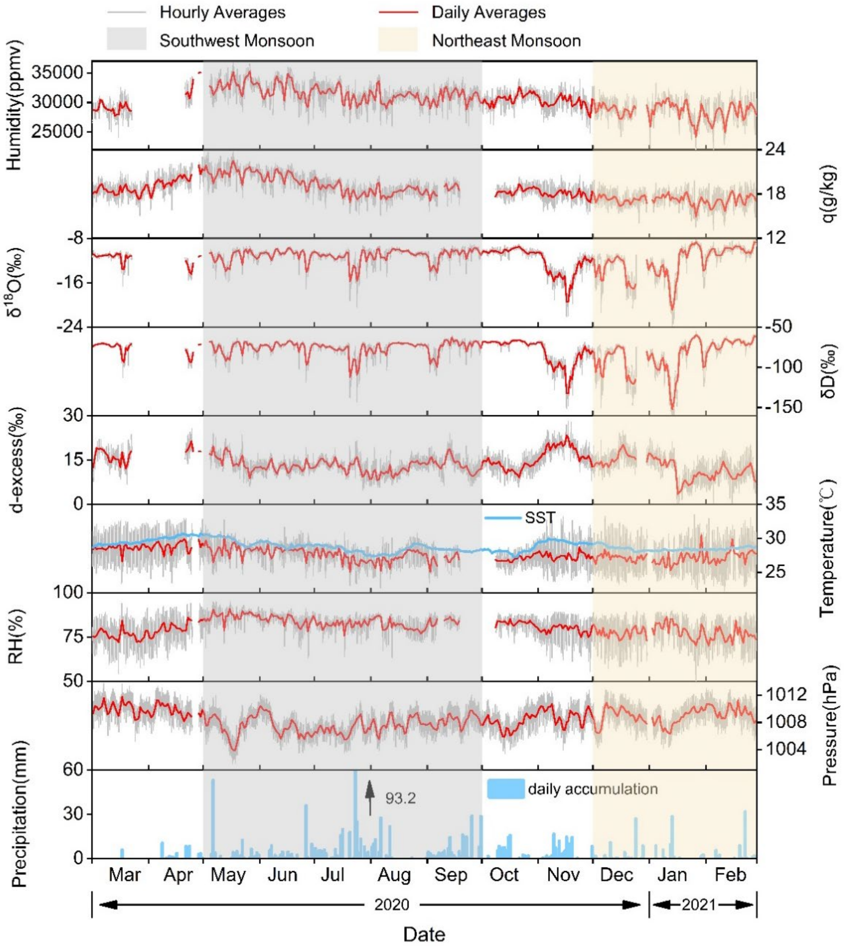

Figure 2: Near-surface observations at the Matara station depict water vapor isotopes ($\delta^{18}O$, δD, and d-excess) alongside local meteorological parameters (humidity, specific humidity (q), temperature, relative humidity (RH), pressure, and precipitation) during non-monsoon, southwest monsoon, and northeast monsoon periods from March 1, 2020, to February 28, 2021. As Matara is a coastal city, local sea surface temperature (SST) is also plotted in blue.

Table 1: Summary of hourly-averaged data at Matara station during monsoon and non-monsoon periods from March 1, 2020, to February 28, 2021, including averages (bold), standard deviations (SD), minima, maxima, and the number of values (N) for $\delta^{18}O$, δD, d-excess, temperature (T), relative humidity (RH), specific humidity (q), atmospheric boundary layer height (BLH), and lifting condensation level (LCL). The maximum and minimum value for the year is all highlighted in bold italics.

Season		$\delta^{18}O$	δD	d-excess	T	RH	q	BLH	LCL
		(‰)	(‰)	(‰)	(°C)	(%)	(g/kg)	(m)	(m)
Non-monsoon	mean	**-11.9**	**-80.6**	**14.7**	**28.0**	**79.4**	**18.6**	**630.1**	**471.4**
	SD	2.2	16.6	3.8	2.2	7.3	1.3	179.1	204.1
	Max.	-9.0	-65.3	***28.1***	33.2	94.2	23.0	1178.8	1283.1
	Min.	-22.1	-151.1	5.1	23.3	54.2	15.1	***84.4***	98.1
	N	1851	1851	1851	2617	2617	2617	2928	2617
Southwest monsoon	mean	**-11.1**	**-75.7**	**13.0**	**27.6**	**83.8**	**19.4**	**741.4**	**348.7**
	SD	1.3	9.6	2.8	1.5	4.5	1.5	149.0	118.4
	Max.	-9.1	-60.8	24.1	32.7	***95.0***	***23.7***	***1564.4***	938.9
	Min.	-20.4	-143.5	4.5	22.7	63.4	15.1	259.0	***78.5***
	N	3314	3314	3314	3192	3197	3192	3672	3192
Northeast monsoon	mean	**-12.2**	**-85.1**	**12.4**	**27.1**	**77.4**	**17.2**	**516.4**	**524.7**
	SD	3.0	22.0	4.29	2.4	7.8	1.2	139.4	224.0
	Max.	***-7.5***	***-53.4***	25.0	***33.5***	90.0	19.9	1125.7	***1465.6***
	Min.	***-23.9***	***-173.2***	***-1.2***	***22.3***	***49.2***	***13.1***	182.0	192.3
	N	1885	1885	1885	1993	1993	1993	2160	1993
All	mean	**-11.6**	**-79.5**	**13.3**	**27.6**	**80.7**	**18.6**	**648.7**	**434.8**
	SD	2.2	16.1	3.6	2.0	7.0	2.1	181.3	195.1
	Max.	-7.5	-53.4	28.1	33.5	95.0	23.7	1564.4	1465.6
	Min.	-23.9	-173.2	-1.2	22.3	49.2	13.1	84.4	78.5
	N	7050	7050	7050	7802	7807	7807	8760	7802

For δ^{18}O, δD, and d-excess, synoptic variations are also recorded (Fig. 2). Abrupt changes occur in late July 2020 and from November 2020 to January 2021, associated with synoptic events. Cumulative precipitation for July 2020 reached 451.8 mm, with a notable rainfall event in late July recording daily rainfall of 93.2 mm. Isotopic δ^{18}O values emerged a sharp depletion from -10.4‰ to -20.4‰ within 20 hours during isolated rainfall events. This depletion process of isotopes lasted for 6 days. Over a 75-day period spanning from late southwest monsoon to mid-northeast monsoon, noticeable fluctuations in isotopic δ values range from -22‰ to -11‰. during the southwest monsoon from July 12 to August 7, δ^{18}O values varied from -20.4‰ to -9.2‰, and δD values ranged from -143.5‰ to -68.6‰. This finding is consistent with water vapor isotopic δ^{18}O (-14.1‰ to -9.8‰) and δD (-97.2‰ to 69.1‰) values measured from July 12 to August 7, 2012, near the Bay of Bengal, although the local minimum at Matara station is below the minimum in the Bay of Bengal (Midhun et al., 2013). Stations such as Bangalore, Ponmudi, and Wayanad, all coastal like Matara, exhibit water vapor isotopic values deficient in autumn and winter, mirroring observations at Matara station (Table 2).

The atmospheric water vapor line serves as an indicator of the humidity conditions at the vapor source and the fractionation processes along the transport path. The slope reflects the extent of kinetic fractionation the vapor has experienced, while the intercept indicates the humidity levels at the vapor source. Local Meteoric Water Line (LMWL) for δ^{18}O and δD, compared with the Global Meteoric Water Line (GMWL), shows a slope of < 8 during both monsoon periods (Fig. 3a). Seasonal variations are also visible in δ^{18}O and δD distribution patterns. Daily averages of water vapor isotopic δ^{18}O and δD demonstrate a strong correlation ($r = 0.96$) with a slope of 7.26 with a lower intercept of 4.68. During the northeast monsoon, LMWL slope and intercept are higher compared to other periods, indicating significant moisture recirculation. During The southwest monsoon, lower slope (6.93) and intercept (1.18) are exhibited compared to other periods, correlating with higher rainfall (Fig. 2).

https://doi.org/10.5194/egusphere-2024-1840
Preprint. Discussion started: 5 August 2024

Table 2: Summary of observed water vapor isotope concentrations at various stations in India and the Bay of Bengal, showing variations within each period.

Country or region	Station or location	Latitude (N°)	Longitude (E°)	Date	$\delta^{18}O$ (‰)	δD (‰)	d-excess (‰)	References
India	Bangalore	13.01	77.55	Jun 1, 2012, to Sep 30, 2012	-23.8 to -9.0	-178.3 to -58.6	-4.5 to 32.7	(Rahul et al., 2016b)
				Oct 1, 2012, to Feb 28, 2013	-22.7 to -10.2	-177.1 to -73.7	-9.5 to 41.4	
	Kolkata	22.56	88.41	May 3, 2019, to Oct 25, 2019	-16.9 to -10.0	-128.3 to -72.8	-7.1 to 25.4	(Bhattacharya et al., 2021)
	Roorkee	29.87	77.88	Feb 1, 2007, to May 31, 2007	-17.0 to -3.0	none	32.0 to 70.0	(Saranya et al., 2018)
				Jun 1, 2007, to Sep 30, 2007	-32.0 to -6.0		40.0 to 87.0	
				Oct 1, 2007, to Dec 31, 2007	-30.0 to -7.0		30.0 to 60.0	
	Ponmudi	8.76	77.12	Apr 1, 2012, to Nov 30 2012	-24.1 to -8.6	-170.0 to -51.0	6.3 to 26.5	(Lekshmy et al., 2018)
	Wayanad	11.51	76.02		-20.5 to -7.9	-139.1 to -50.0	13.3 to 31.2	
	Ahmedabad	23.03	72.56	Apr 1, 2007, to Apr 1, 2008	-19.2 to -8.9	-128.1 to -59.8	6.9 to 40.4	(Srivastava et al., 2015)
	Chhota Shigri	32.58	77.58	none	-19.4 to -10.3	-101.5 to -29.2	28.0 to 62.0	(Ranjan et al., 2021)
Bay of Bengal	6m	none		Jul 1, 2012, to Aug 1, 2012	-13.6 to -10.0	-94.0 to -68.3	5.7 to 16.4	(Midhun et al., 2013)
	25m				-14.1 to -9.8	-97.2 to -69.1	6.9 to 19.4	
	25m			Nov 15, 2013, to Dec 1, 2013	-19.9 to -11.0	-136.6 to -69.4	13.3 to 31.0	(Lekshmy et al., 2022)

The observation period revealed a significant negative relationship between d-excess and $\delta^{18}O$, where the rate of change for d-excess with $\delta^{18}O$ is -0.68 ‰/‰ ($r = -0.55$) (Fig. S4a), which is below the -1.4 ‰/‰ recorded at the southern Greenland Ivittuut station and the -1.2~ -1.1 ‰/‰ range observed at NEEM station during the summer (Steen-Larsen et al., 2013b; Bonne et al. 2014). Seasonally, the correlation between the two variables weakens sequentially during the southwest monsoon period, northeast monsoon period, and the non-monsoon period. The rates of change are -0.94 ‰/‰ (r = -0.49), -0.69 ‰/‰ (r = -0.54), and -0.65 ‰/‰ (r = -0.44), respectively. Similar patterns are detected for temperature–d-excess and specific humidity–d-excess correlations. This pattern aligns with the incremental rise in the slope and intercept of the water vapor line. Moreover, the concentrated distribution of vapor values during the southwest monsoon and the highly scattered distribution during the northeast monsoon are indicative of the corresponding seasonal distributions of the water vapor line.

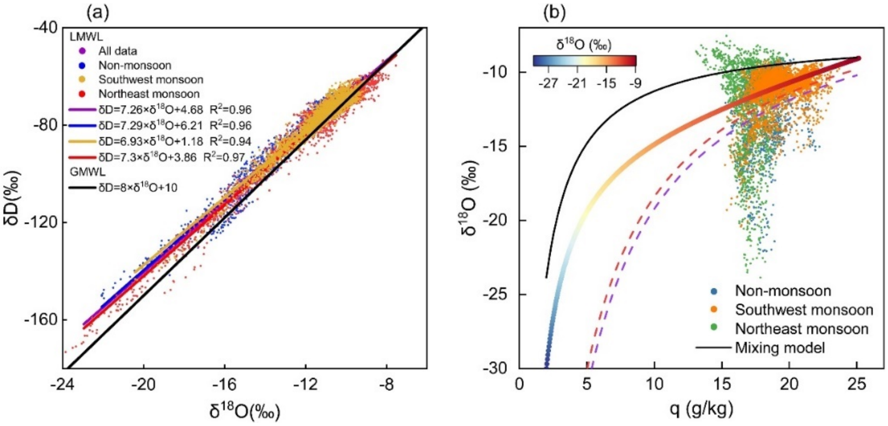

Figure 3: (a) Co-variation of water vapor isotopic composition and meteorological parameters during different monsoon and non-monsoon periods from March 1, 2020, to February 28, 2021. The lines represent linear least-squares regressions (LMWL and GMWL) of δD (‰) as a function of δ^{18}O (‰). (b) Scatter plot of observed hourly water vapor isotopic δ^{18}O vs. specific humidity (q). The dotted red curve represents the Rayleigh distillation line during the southwest monsoon. The dotted blue curve represents the Rayleigh distillation line during the northeast monsoon. The solid black curve represents the mixing line. The colorful curve represents the MBL-mix line.

The q-δ^{18}O plots, combined with theoretical Rayleigh distillation curve, mixing curve, and MBL-mix curve, were utilized to assess mixing conditions during the studied periods (Fig. 3b). During the southwest monsoon, most measurements are clustered between the Rayleigh curve and mixing curve, indicating isotopic variability dominated by precipitation leaching process and moisture mixing process. Limited water vapor

https://doi.org/10.5194/egusphere-2024-1840
Preprint. Discussion started: 5 August 2024

measurements are scattered below the Rayleigh fractionation line, implying a discernible impact of raindrop re-evaporation. Similarly, during the non-monsoon period, most measurements are observed between the Rayleigh curve and mixing curve, with a few located below the Rayleigh line. During the northeast monsoon, $\delta^{18}O$ spans both upper and lower sides of the mixing curve and Rayleigh distillation curve. The measurements substantially deviated from the Rayleigh curve and more depleted than Rayleigh prediction, which is likely due to the influence of convective processes.

3.2 Diurnal Cycles

To evaluate diurnal cycles in isotopic composition and meteorological parameters, we analyzed hourly averages at Matara station, particularly focusing on the pronounced diurnal patterns during the northeast monsoon characterized by stable weather conditions (low horizontal wind speed) (Fig. 4c-e).

All water vapor isotopic signals ($\delta^{18}O$, δD, and d-excess) and meteorological parameters exhibit strong diurnal variations during both monsoon and non-monsoon periods (Fig. 4). Overall, the diurnal variation of local meteorological factors reflects the dynamic changes in the atmospheric boundary layer at Matara. During the daytime, as solar radiation intensifies and the boundary layer develops, temperatures and wind speeds increase from noon to afternoon, accompanied by a decrease in relative humidity and led to significant evapotranspiration. At night, surface radiative cooling causes temperatures to drop, resulting in near-surface calm conditions and gradual air saturation, which points to a relatively stable atmospheric boundary layer. During the southwest monsoon, $\delta^{18}O$, δD, relative humidity, wind speed, specific humidity, and BLH are generally higher than the northeast monsoon and non-monsoon periods, while d-excess and LCL are lower. In the early morning, $\delta^{18}O$ values steadily drop, reaching their lowest level (-11.26‰) at around sunrise (~09:00 local time (LT)). Subsequently, they increase throughout the day, peaking (-10.87‰) in the afternoon (~15:00 LT), with a diurnal fluctuation of merely 0.45‰. Increased specific humidity between 10:00 LT and 14:00 LT coincides with rises in air temperature and wind speed and a decline in relative humidity (Fig. 4c-f). BLH peaks between 14:00 LT and 16:00 LT, slightly

https://doi.org/10.5194/egusphere-2024-1840
Preprint. Discussion started: 5 August 2024

delayed compared to other meteorological parameters. Conversely, the northeast monsoon exhibits reversed diurnal variations for each parameter. During the northeast monsoon, the daily variations of $\delta^{18}O$ and d-excess are significant, with the maximum amplitude changes at 1.1‰ and 6.8‰, respectively. Specific humidity peaks from 10:00 LT to 16:00 LT, accompanied by increases in air temperature, wind speed, BLH, and LCL. After 16:00 LT, specific humidity decreases alongside declines in isotopic δ values and other meteorological parameters. The d-excess peaks (14.81‰) at 09:00 LT and fluctuates until 23:00 LT, contrasting with the period from 04:00 LT to 09:00 LT (Fig. 4b). The d-excess exhibits a W-shaped variability, reaching similar highs at 09:00 LT and 21:00 LT. Specific humidity exhibits a diurnal variation that aligns closely with the $\delta^{18}O$ pattern, reaching its minimum before sunrise and peaking around midday (10:00-15:00 LT). From the afternoon to evening, specific humidity stays relatively high and stable. The diurnal variation during the southwest monsoon and northeast monsoon periods is 1.28 g/kg and 2.32 g/kg, respectively. Similarities with Lena station patterns (Bonne et al. 2020) suggest potential influences from moisture exchange between the atmosphere and the ocean surface, particularly during the northeast monsoon.

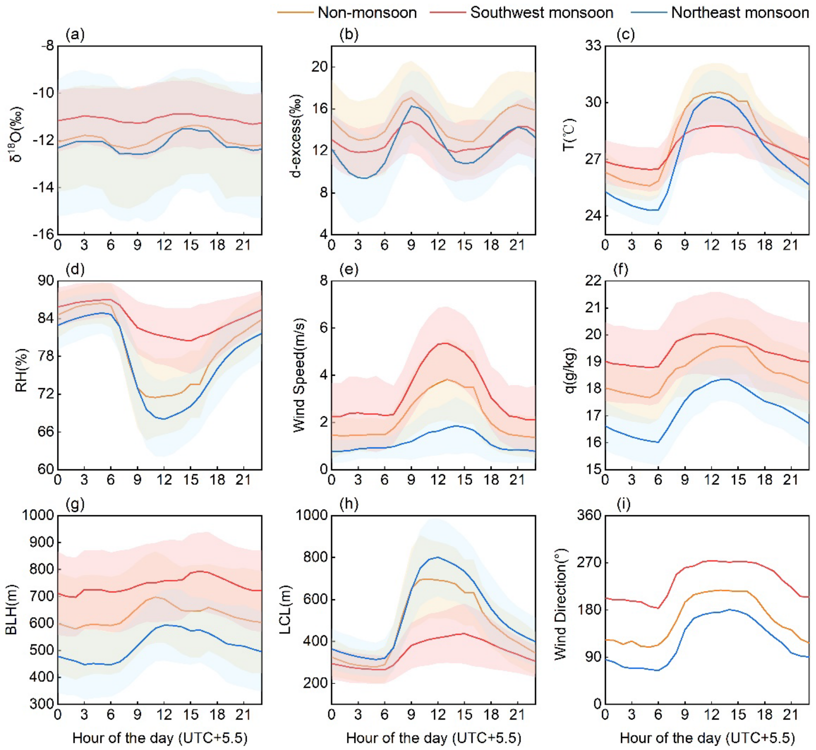

Figure 4: Depicts average diurnal cycles of (a) δ^{18}O, (b) d-excess, (c) temperature (T), (d) relative humidity (RH), (e) wind speed, (f) specific humidity (q), (g) atmospheric boundary layer height (BLH), (h) lifting condensation level (LCL), and (i) wind direction during the non-monsoon, southwest monsoon, and northeast monsoon periods. Shaded areas correspond to ±1 standard deviation.

3.3 Sea Surface Evaporation Conditions in the Moisture Source Region

Understanding the processes and factors influencing water stable isotopic variations in ocean evaporation is crucial for exploring water vapor isotopic variations in the sea surface boundary layer. The primary determinant governing water vapor stable isotope shifts across different regions is the regional moisture transport process, characterized by differences in isotopic variations in the moisture source region, variations in meteorological conditions during evaporation processes, and divergences

https://doi.org/10.5194/egusphere-2024-1840
Preprint. Discussion started: 5 August 2024

of moisture transport pathways (Bonne et al., 2020). Thus, this section aims to reveal essential factors driving the seasonal variation of near-surface atmospheric water vapor stable isotopes at Matara, including water vapor origins, transmission routes, and sea surface evaporation conditions in the source regions.

To further understand the different seasonal relationships between δ^{18}O, d-excess, and meteorological parameters, we analyzed potential seasonal differences in the main moisture sources for water vapor transported to Matara Station during the 2020-2021 southwest monsoon and northeast monsoon by HYSPLIT. Trajectories during the southwest monsoon and northeast monsoon show different origins of water vapor. During the southwest monsoon, origins are mostly in the Arabian Sea (AS) and Indian Ocean due to the northward movement of the warm South Equatorial Current, bringing heavy rainfall to Matara. Conversely, during the northeast monsoon, most trajectories originate in northeast India with lower specific humidity due to overland airflow, and a small part from the BoB. The long transport distance results in more depletion of water vapor isotopes at Matara station.

We calculated water vapor sources at Matara station for each month during the two monsoon seasons. Fig. 5a shows that the primary moisture sources are the Indian Ocean to the southwest and the BoB to the northeast of Matara. During the southwest monsoon, water vapor predominantly originates from the Indian Ocean, encompassing wind directions spanning 60° to 360°. Conversely, during the northeast monsoon, the primary water vapor source shifts to the BoB, featuring wind directions from 0° to 225° and 330° to 360° to exclude the influence of inland water vapor. Moisture from all sources shows seasonal variations, with depleted δ^{18}O values during the southwest monsoon and enriched δ^{18}O values during the northeast monsoon. The shift in water vapor source from the AS to the southern Indian Ocean between May and September leads to enriched water vapor δ^{18}O values from August to September. Enhanced convective activity and rainfall during the southwest monsoon result in δ^{18}O depletion, while tropical storms and hurricanes also contribute to δ^{18}O depletion.

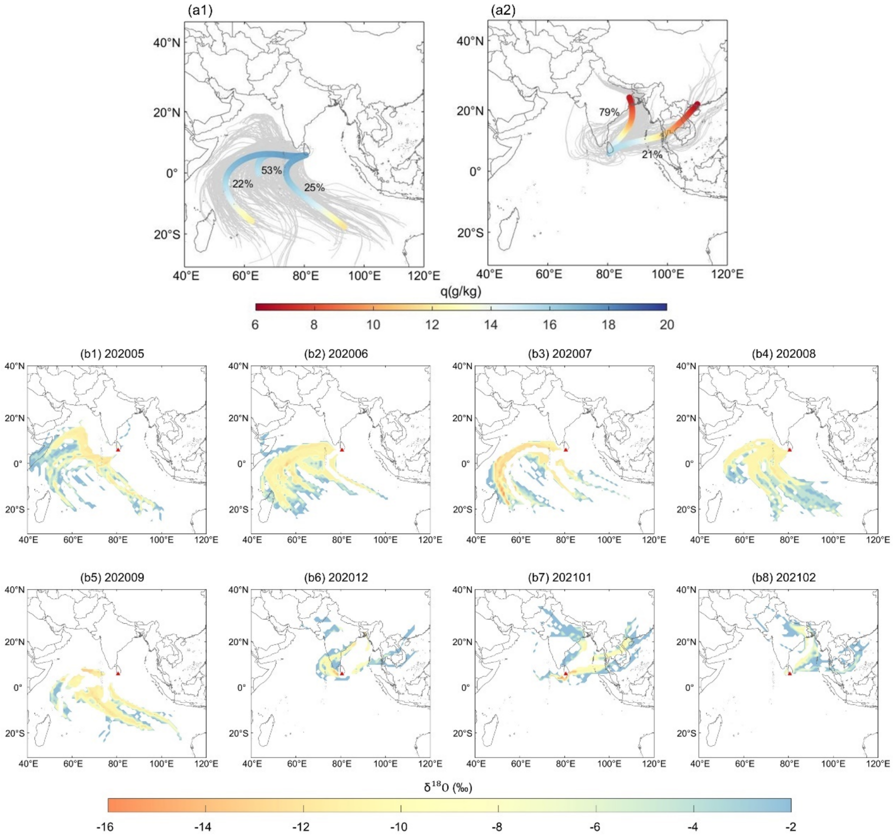

Figure 5: Backward trajectories of water vapor tracks reaching Matara station (height of 50m) during (a) southwest monsoon and (b) northeast monsoon. The changes in specific humidity (q) along each clustered trajectory are shown in color. The black numbers indicate the percentages, reflecting the proportion of each clustered trajectory. Monthly concentration fields of water vapor isotopic δ^{18}O for 168h HYSPLIT back trajectories during the two monsoons (b1-b8). Red triangle marks the study site.

Similar seasonal variations are observed in d-excess values at Matara station, with lower values during the two monsoon seasons and higher values in the non-monsoon periods (refer to Table 2, Fig. 4). This seasonal variation in d-excess may stem from changes in relative humidity in the moisture source areas and further modifications during moisture transport.

Previous observational studies in the marine boundary layer have confirmed a

https://doi.org/10.5194/egusphere-2024-1840
Preprint. Discussion started: 5 August 2024

significant association between d-excess monitored at coastal observation stations and RH_{SST} in the proximate oceanic source areas (Pfahl and Wernli, 2009; Steen-Larsen et al., 2015). During the southwest monsoon, RH_{SST} values in "region a" ranged from 66% to 84%, with SST fluctuating between 28.0°C and 30.6°C. During the northeast monsoon, RH_{SST} values in "region b" ranged from 54% to 84%, with SST fluctuating between 28.1°C and 29.1°C. In comparison with the southwest monsoon, RH_{SST} exhibits a comparatively drier tendency, accompanied by less pronounced variability in SST. The rate of change in d-excess under the influence of RH_{SST} in the BoB (during the northeast monsoon) is -0.34 ‰/%. In comparison, the rate of change in d-excess with the RH_{SST} of the northern Indian Ocean (during the southwest monsoon) is -0.51 ‰/%, suggesting that the evaporation from the northern Indian Ocean significantly impacts local d-excess. Studies focused on the sea surface of BoB reveal that RH_{SST} explains only 25% of the d-excess variation (d-excess = $(-0.55 \pm 0.14) \times RH_{SST} + (56 \pm 12)$; $r = -0.5$). The limited variation in relative humidity during the monsoon period diminish the correlation, indicating that monsoon moisture plays a crucial role in the isotopic composition of water vapor in the BoB (Midhun et al., 2013). Conversely, the observed relationship between near-surface water vapor d-excess at Matara and relative humidity in the surrounding oceanic region during the observational period, with correlation coefficients of -0.61 and -0.62 ($p<0.01$), respectively (Fig. 6) reveals a marked negative correlation between d-excess and relative humidity in the nearby Indian Ocean and BoB, indicating that water vapor at Matara is predominantly supplied by the adjacent marine environment. Notably, SST amplitude near the Matara station is smaller than the near-surface air temperature, as depicted by the SST line in Fig. 2.

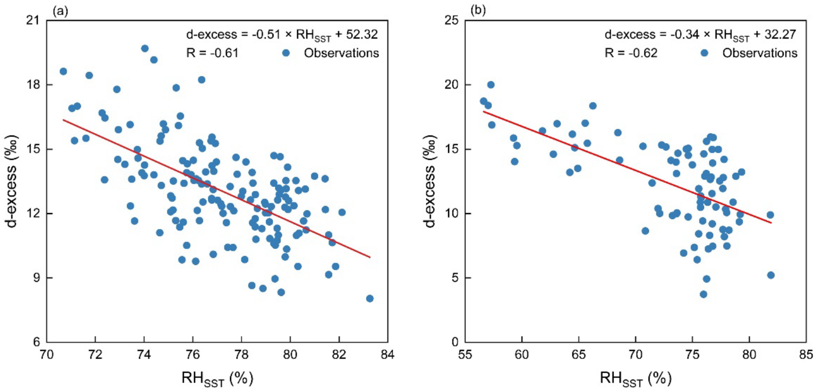

Figure 6: illustrates the relationship between d-excess and RH_{SST} during the (a) southwest monsoon and (b) northeast monsoon. Specific sea regions (Fig. S6) to the south (Region a: 3-6°N and 78-82°E) and east (Region b: 6-8°N and 82-85°E) of the observation station were selected to investigate the impact of sea surface meteorological conditions on near-surface water vapor isotopes during the two monsoon periods.

3.4 Influence of Convective Activity

In the equatorial tropics, OLR mainly results from convective activity and cloud cover, which can impact the stable isotopic composition of precipitation (Ohring et al., 1984; Gao et al., 2013; Guo et al., 2017). Generally, higher OLR values are associated with weaker convective activity. Examining the correlation between stable isotopes of water vapor and OLR helps to understand the impact of convective activities along near-surface trajectories of water vapor stable isotopes at Matara station.

We calculate the spatiotemporal correlation of OLR, and precipitation amount with the measured water vapor isotopic compositions at Matara station, covering the period from March 2020 to February 2021. For each grid point in this region, we calculate the average precipitation amount by averaging over different numbers of days (n = 1, 2, up to 30) preceding each precipitation day. Lower OLR values represent the presence of deep convective clouds in this region, indicating relatively higher precipitation and associated with lower δ values.

Figure 7a represents the strong positive correlation (red regions) between rainfall and $\delta^{18}O$ during the southwest monsoon, mainly in the north BoB and India. This

https://doi.org/10.5194/egusphere-2024-1840
Preprint. Discussion started: 5 August 2024

correlation strengthens and extends over wider areas as n increases from 1 to 5. Additionally, a strong negative correlation is evident in the northern Indian Ocean and southern Arabian Sea, with correlations reaching a maximum for n = 2 days. During the northeast monsoon, the spatial correlation distribution differs, with a negative correlation observed in the southern Indian Ocean and BoB (Fig. 7b). Lower OLR values in the Arabian Sea, the southern part of the BoB, and throughout Southeast Asia correspond to a decrease in water vapor isotopic δ^{18}O at Matara station (Fig. 7c, d). This pattern indicates that water vapor δ^{18}O during the northeast monsoon period is influenced by convective activities in the Arabian Sea, South BoB, and Southeast Asian regions. The stronger the convective activity, the more depleted water vapor isotopic δ^{18}O the air reaching Matara becomes.

To examine the correlation between water vapor isotopic δ^{18}O and local precipitation (Fig. 7e) and OLR (Fig. 7f), we choose a small region of 5°×5° with Matara and calculate the time- and space- correlation for all grid points as described above. The results show that the correlation with precipitation is negative during both monsoon seasons as expected. The depletion of low-level water vapor δ^{18}O is related to the transport and deposition of water vapor into the lower atmosphere through convective activity (Kurita, 2013; Midhun et al., 2013; Lekshmy et al., 2014). The air masses are re-supplied to the convective system through moisture recycling. This results in a strong correlation between the isotopic composition of water vapor and the convective activity of the previous day Fig. 7e and 7f. The residual water vapor is more depleted in strong convective systems. In our study, the correlation reaches a high value after about 5 days, indicating that the convective activity is sufficiently established to affect the isotopic composition of water vapor. the correlation (for $p < 0.05$ and in absolute terms) is indeed high for all n values, with maxima of about 0.48 for n = 3 days during the southwest monsoon and about 0.72 for n = 4 to 9 days during the northeast monsoon.

The OLR correlation peaks at smaller time scales (refer to Fig. 7f), approximately 1-4 days, in contrast to precipitation, which peaks over larger time scales of 3-8 days.

We attribute this difference to the effect of cloud distribution on precipitation and OLR. OLR has a stronger response to shallow clouds, while precipitation is more responsive to both deep convective clouds and shallow clouds (Masunaga and Kummerow, 2006; Schumacher, 2006). The OLR minimum occurs when thunderstorm clouds result in more precipitation. Additionally, deep thunderstorm clouds, with short lifetimes and consequently very low OLR (corresponding to highly depleted water vapor isotopic δ), exhibit a short memory effect on the correlation (peak occurs at smaller time scales) (Gambheer and Bhat, 2000).

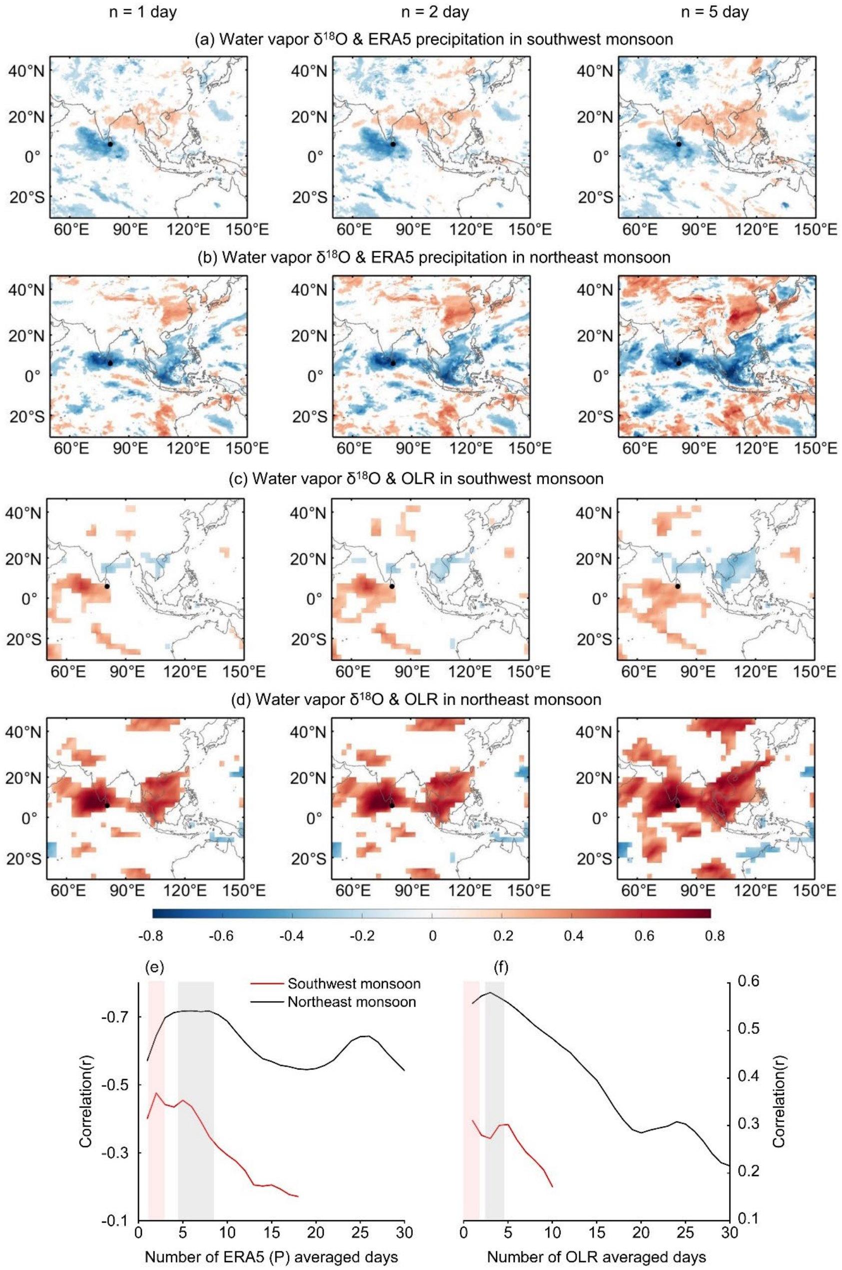

Figure 7: Spatial correlation fields of water vapor isotopic composition and averaged ERA5 precipitation (P) during the (a) southwest monsoon and (b) northeast monsoon, along with the spatial correlation field of average outgoing longwave radiation (OLR) during the (c) southwest monsoon and (d) northeast monsoon. Averaging was conducted at each grid point

https://doi.org/10.5194/egusphere-2024-1840
Preprint. Discussion started: 5 August 2024

for three periods of n = 1, 2, and 5 days preceding each of the 153 days of the southwest monsoon (a, c) and 90 days of the northeast monsoon (b, d). Correlation between $\delta^{18}O$ and (e) P, along with (f) OLR during the southwest monsoon (red line) and northeast monsoon (black line) for values over n days (n = 1, 2, 3, … 30). Red (grey) area shows n-range with highest correlation during southwest monsoon (northeast monsoon). Here, n represents the average "moisture mixing time" of regional precipitation, affecting water vapor isotopes through the transport of residual water vapor (Rahul et al., 2016b).

During both the southwest and northeast monsoons, $\delta^{18}O$ exhibits weak correlation with 2m air temperature (Fig. S7). Throughout the year, the relationship between 2m air temperature and $\delta^{18}O$ in water vapor is $\delta^{18}O = 0.7T - 30.8$ (r = 0.32) (Fig. S9). During the southwest and northeast monsoons, the relationships become $\delta^{18}O = 0.5T - 24.95$ (r = 0.39) and $\delta^{18}O = 1.46{*}T - 51.71$ (r = 0.43), respectively (Fig. S7). Daily temperature and $\delta^{18}O$ values fluctuate less during the southwest monsoon than in the northeast monsoon period (Fig. 4), possibly due to a weaker temperature inversion during the southwest monsoon.

The correlation between $\delta^{18}O$ and relative humidity differs between the two monsoon periods. During the southwest monsoon, $\delta^{18}O$ and relative humidity appear uncorrelated (r = 0.01), consistent with previous findings (Rahul et al., 2016b). Conversely, during the northeast monsoon, a robust negative correlation emerges between $\delta^{18}O$ and relative humidity (r = -0.58). Similarly, the relationship between $\delta^{18}O$ and precipitation varies between both monsoon seasons (Fig. S7). During the southwest monsoon, heavy precipitation leads to relatively high relative humidity and the enrichment of heavier isotopes.

4. Summary and conclusions

This study presents one-year (March 2020 to February 2021) in-situ observations of near-surface atmospheric water vapor isotopes ($\delta^{18}O$, δD) at Matara station in Sri Lanka. These high-temporal resolution water vapor isotopic composition and meteorological observations at Matara station provide a new sight to investigate the water vapor isotopic dynamics from synoptic scale to seasonal scale. The variability of water vapor isotopes at Matara station is influenced by local meteorological factors, oceanic evaporation processes, and regional convective activities, depending on the water sources and moisture transport. This dataset provides insights into multi-time-scale variations in near-surface atmospheric water vapor in equatorial regions, and provides information about the interactions between large-scale atmospheric moisture transport and ocean evaporation.

Meteorological parameters exhibit diurnal variations during both monsoon and non-monsoon periods. During the northeast monsoon, the diurnal fluctuation in $\delta^{18}O$, temperature, and specific humidity are observed, with maximum values reaching 1.1‰, 6.0°C, and 2.3 g/kg, respectively. In contrast, variations of these parameters exhibit small magnitude of 0.45‰, 2.3°C, and 1.3 g/kg during the southwest monsoon period. Atmospheric temperature affects isotopic composition through its effect on isotope fractionation. Additionally, a weak seasonal variability in near-surface water vapor isotopes is observed, with $\delta^{18}O$ typically showing high values (-11.1‰) during the monsoon period and low values (-11.9‰) during the non-monsoon period. The d-excess exhibits the lower value (12.7‰) during the monsoon period than that (14.7‰) during the non-monsoon period.

The evaporation from the northern Indian Ocean significantly impacts local d-excess. Contrary to previous research indicating a weak correlation (r = -0.5) between d-excess in the Bay of Bengal and the sea surface relative humidity (RH_{SST}) (Midhun et al., 2013), d-excess at Matara station exhibits a significantly negative correlation with the RH_{SST} during the monsoon periods, with the correlation of -0.61 and -0.62 ($p<0.01$) in the northern Indian Ocean and the Bay of Bengal, respectively. This study underscores the capability of near-surface d-excess to reflect the evaporation conditions over these oceanic regions.

Consistent with previous research (Rahul et al., 2016b), large-scale rainfall and regional convective activity (OLR) significantly impact isotope ratios at Matara station. Notably, significant changes in $\delta^{18}O$ are observed during a heavy rainfall event in July

https://doi.org/10.5194/egusphere-2024-1840
Preprint. Discussion started: 5 August 2024

2020, with a sharp decline in isotopic values from -10.4‰ to -20.4‰ within 20 hours. During the southwest monsoon, strong cloud cover and high humidity over the ocean may lead to $\delta^{18}O$ enrichment at the Matara station. The water vapor isotope compositions observed during the southwest monsoon are similar as those observed in the Bay of Bengal (Midhun et al., 2013). The deficiency of water vapor isotope values at Matara station in autumn and winter is consistent with findings from other coastal stations, such as Bangalore, Ponmudi, and Wayanad (Rahul et al., 2016b; Lekshmy et al., 2018). Our results first pointed out that the correlation between OLR and $\delta^{18}O$ peaks around 1-4 days, attributed to the impacts of cloud distribution.

This study contributes to a better understanding of the moisture origins at Matara station and associated atmospheric transport. This combined water vapor isotope and meteorological dataset offers extensive opportunities to further analysis of the typical weather events, atmospheric patterns and ocean-atmosphere interactions in the equatorial region. Ongoing observations of water vapor stable isotopes in this region are strongly needed. This will support studies on interannual variability. Given the anticipated numerous weather processes and hydrological changes in equatorial regions, future research should explore the impacts of typical weather events, and ocean-atmosphere interactions, deepening our understanding of extreme events and large-scale atmospheric modes (e.g., ENSO, MJO, and IOD). Considering the temporal and spatial variability in the interaction of tropical ocean-atmosphere systems, high-resolution isotope model or satellite observation datasets should be employed for more comprehensive analysis in the future.

Acknowledgements:

This work was funded by The Second Tibetan Plateau Scientific Expedition and Research (STEP) program (Grant No. 2019QZKK0208) and the National Natural Science Foundation of China (Grants 41988101-03 and 41922002), as well as the Innovation Program for Young Scholars of TPESER (QNCX2022ZD-01). We thank staff in the China Sri Lanka Joint Center for Education and Research, Mr. Charith Madusanka Widanage, and Dr. Di Dai for their invaluable support and assistance with measurements.

Author Contributions:

Yuqing Wu: Data curation, Formal analysis, Writing - Original draft preparation. **Jing Gao:** Data curation, Conceptualization, Methodology, Supervision, Writing - Review and Editing, Funding acquisition. **Aibin Zhao**: Writing - Review and Editing, Project administration. **Xiaowei Niu:** Data curation. **Yigang Liu:** Data curation. **Disna Ratnasekera:** Project administration. **Tilak Priyadarshana Gamage:** Project administration. **Amarasinghe Hewage Ruwan Samantha:** Data curation.

Data availability:

The ERA5 dataset is the latest reanalysis dataset published by the European Centre for Medium-Range Weather Forecasts (ECMWF) (Hersbach et al., 2020) (https://cds.climate.copernicus.eu/cdsapp#!/home). The Global Data Assimilation System (GDAS) published by the US National Oceanic and Atmospheric Administration (NOAA) (ftp://arlftp.arlhq.noaa.gov/archives/gdas1/). The water vapor isotopic compositions dataset will be available on the Zenodo research data repository after manuscript publication.

Competing interests:

The contact author has declared that none of the authors has any competing interests.

References

Aemisegger, F., Sturm, P., Graf, P., Sodemann, H., Pfahl, S., Knohl, A., and Wernli, H.: Measuring variations of $\delta^{18}O$ and $\delta^{2}H$ in atmospheric water vapour using two commercial laser-based spectrometers: an instrument characterisation study, Atmos. Meas. Tech., 5, 1491-1511, https://doi.org/10.5194/amt-5-1491-2012, 2012.

Angert, A., Lee, J.E., and Yakir, D.: Seasonal variations in the isotopic composition of near-surface water vapour in the eastern Mediterranean, Tellus B, 60, 674-684, https://doi.org/10.1111/j.1600-0889.2008.00357.x, 2008.

Bailey, A., Aemisegger, F., Villiger, L., Los, S.A., Reverdin, G., Quiñones Meléndez, E., Acquistapace, C., Baranowski, D.B., Böck, T., Bony, S., Bordsdorff, T., Coffman, D., de Szoeke, S.P., Diekmann, C.J., Dütsch, M., Ertl, B., Galewsky, J., Henze, D., Makuch, P., Noone, D., Quinn, P.K., Rösch, M., Schneider, A., Schneider, M., Speich, S., Stevens, B., and Thompson, E.J.: Isotopic measurements in water vapor, precipitation, and seawater during EUREC4A, Earth Syst. Sci. Data, 15, 465-495, https://doi.org/10.5194/essd-15-465-2023, 2023.

Bandara, U., Agarwal, A., Srinivasan, G., Shanmugasundaram, J., and Jayawardena, I.M.S.: Intercomparison of gridded precipitation datasets for prospective hydrological applications in Sri Lanka, Int. J. Climatol., 42, 3378-3396, https://doi.org/10.1002/joc.7421, 2022.

Bavadekar, S.N., and Mooley, D.A.: Use of the equation of continuity of water vapour for computation of average precipitation over peninsular India during the summer monsoon, In: Lighthill, J., Pearce, P.R. (Eds.), Monsoon Dynamics, Cambridge University Press, Cambridge, pp., 261-268, 1981.

Bedaso, Z., and Wu, S-Y.: Daily precipitation isotope variation in Midwestern United States: Implication for hydroclimate and moisture source, Sci. Total Environ., 713, 136631, https://doi.org/10.1016/j.scitotenv.2020.136631, 2020.

Benetti, M., Aloisi, G., Reverdin, G., Risi, C., and Sèze, G.: Importance of boundary layer mixing for the isotopic composition of surface vapor over the subtropical North Atlantic Ocean, J. Geophys. Res. Atmos., 120, 2190-2209, https://doi.org/10.1002/2014JD021947, 2015.

Benetti, M., Lacour, J-L., Sveinbjörnsdóttir, A.E., Aloisi, G., Reverdin, G., Risi, C., Peters, A.J., and Steen-Larsen, H.C.: A Framework to Study Mixing Processes in the Marine Boundary Layer Using Water Vapor Isotope Measurements, Geophys. Res. Lett., 45(5), 2524-2532, https://doi.org/10.1002/2018GL077167, 2018.

Benetti, M., Reverfdin, G., Pierre, C., Merlivat, L., Risi, C., Steen-Larsen, H.C., and Vimeux, F.: Deuterium excess in marine water vapor: Dependency on relative humidity and surface wind speed during evaporation, J. Geophys. Res. Atmos., 119, 584-593, https://doi.org/10.1002/2013JD020535, 2014.

Bershaw, J., Penny, S.M., and Garzione, C.N.: Stable isotopes of modern water across the Himalaya and eastern Tibetan Plateau: Implications for estimates of paleoelevation and paleoclimate, J. Geophys. Res. Atmos., 117, 110, https://doi.org/10.1029/2011JD016132, 2012.

Bhattacharya, S., Pal, M., Panda, B., and Pradhan, M.: Spectroscopic investigation of hydrogen and triple-oxygen isotopes in atmospheric water vapor and precipitation during Indian monsoon season, Isot. Environ. Healt. S., 57, 368-385, https://doi.org/10.1080/10256016.2021.1931169, 2021.

Bonne, J-L., Behrens, M., Meyer, H., Kipfstuhl, S., Rabe, B., Schönicke, L., Steen-Larsen, H.C., and Werner, M.: Resolving the controls of water vapour isotopes in the Atlantic sector, Nat. Commun., 10, 1632, https://doi.org/10.1038/s41467-019-09242-6, 2019.

Bonne, J-L., Masson-Delmotte, V., Cattani, O., Delmotte, M., Risi, C., Sodemann, H., and Steen-Larsen, H.C.: The isotopic composition of water vapour and precipitation in Ivittuut, Southern Greenland, Atmos. Chem. Phys., 14, 4419-2014, https://doi.org/10.5194/acp-14-4419-2014, 2014.

Bonne, J-L., Meyer, H., Behrens, M., Boike, J., Kipfstuhl, S., Rabe, B., Schmidt, T., Schönicke, L., Steen-Larsen, H.C., and Werner, M.: Moisture origin as a driver of temporal variabilities of the water vapour isotopic composition in the Lena River Delta, Siberia, Atmos. Chem. Phys., 20, 10493-10511, https://doi.org/10.5194/acp-20-10493-2020, 2020.

Bookhagen, B., and Burbank, D.W.: Toward a complete Himalayan hydrological budget: Spatiotemporal distribution of snowmelt and rainfall and their impact on river discharge, J. Geophys. Res., 115, F03019, https://doi.org/10.1029/2009JF001426, 2010.

Cai, Z., Tian, L., and Bowen, G.J.: ENSO variability reflected in precipitation oxygen isotopes across the Asian Summer Monsoon region, Earth Planet. Sci. Lett., 475, 25-33, https://doi.org/10.1016/j.epsl.2017.06.035, 2017.

Cai, Z., and Tian, L.: Atmospheric Controls on Seasonal and Interannual Variations in the Precipitation Isotope in the East Asian Monsoon Region, J. Climate, 29, 1339-1352, https://doi.org/10.1175/JCLI-D-15-0363.1, 2016.

Chakraborty, S., Sinha, N., Chattopadhyay, R., Sengupta, S., Mohan, P.M., and Datye, A.: Atmospheric controls on the precipitation isotopes over the Andaman Islands, Bay of Bengal, Sci. Rep., 6, 19555, https://doi.org/10.1038/srep19555, 2016.

Craig, H.: Isotopic Variation in Meteoric Waters. Science, 133, 1702-1703, https://doi.org/10.1126/science.133.3465.1702, 1961.

Craig, H., and Gordon, L.I.: Deuterium and oxygen 18 variation in the ocean and the marine atmosphere, In: Tongiorgi, E. (Eds.), Stable Isotopes in Oceanographic Studies and Paleotemperatures, pp., 9-130, 1965.

Curry, J.A., and Webster, P.J.: Thermodynamics of Atmospheres and Oceans, Academic Press, London, 31705, 1999.

Dai, D., Gao, J., Steen-Larsen, H.C., Yao, T., Ma, Y., Zhu, M., and Li, S.: Continuous monitoring of the isotopic composition of surface water vapor at Lhasa, southern Tibetan Plateau, Atmos. Res., 264, 105827, https://doi.org/10.1016/j.atmosres.2021.105827, 2021.

Dansgaard, W.F.: Stable Isotopes in Precipitation, Tellus B, 16, 436-468, https://doi.org/10.1111/j.2153-3490.1964.tb00181.x, 1964.

Delattre, H., Vallet-Coulomb, C., and Sonzogni, C.: Deuterium excess in the atmospheric water vapour of a Mediterranean coastal wetland: regional vs. local signatures, Atmos. Chem. Phys., 15, 10167-10181, https://doi.org/10.5194/acp-15-10167-2015, 2015.

de Vries, A.J., Aemisegger, F., Pfahl, S., and Wernli, H.: Stable water isotope signals in tropical ice clouds in the West African monsoon simulated with a regional convection-permitting model, Atmos. Chem. Phys., 22, 8863-8895, https://doi.org/10.5194/acp-22-8863-2022, 2022.

Dhar, O., and Rakhecha, P.: Foreshadowing Northeast Monsoon Rainfall Over Tamil Nadu, India, Mon. Weather Rev., 111, 109, https://doi.org/10.1175/1520-0493(1983)111<0109:FNMROT>2.0.CO;2, 1983.

Diekmann, C.J., Schneider, M., Knippertz, P., de Vries, A.J., Pfahl, S., Aemisegger, F., Dahinden, F., Ertl, B., Khosrawi, F., Wernli, H., and Braesicke, P.: A Lagrangian Perspective on Stable Water Isotopes During the West African Monsoon, J. Geophys. Res. Atmos., 126, e2021JD034895, https://doi.org/10.1029/2021JD034895, 2021.

Dütsch, M., Pfahl, S., Meyer, M., and Wernli, H.: Lagrangian process attribution of isotopic variations in near-surface water vapour in a 30-year regional climate simulation over Europe, Atmos. Chem. Phys., 18, 1653-1669, https://doi.org/10.5194/acp-18-1653-2018, 2018.

Gadgil, S.: The Indian Monsoon and Its Variability, Rev. Earth Pl. Sci., 31, 429-467, https://doi.org/10.1146/annurev.earth.31.100901.141251, 2003.

Galewsky, J., and Hurley, J.V.: An advection-condensation model for subtropical water vapor isotopic ratios, J. Geophys. Res. Atmos., 115, 116, https://doi.org/10.1029/2009JD013651, 2010.

Galewsky, J., Steen-Larsen, H.C., Field, R.D., Worden, J., Risi, C., and Schneider, M.: Stable isotopes in atmospheric water vapor and applications to the hydrologic cyclem, Rev. Geophy., 54, 809-865, https://doi.org/10.1002/2015RG000512, 2016.

Gambheer, A.V., and Bhat, G.S.: Life Cycle Characteristics of Deep Cloud Systems over the Indian Region Using INSAT-1B Pixel Data, Mon. Weather Rev., 128, 4071-4083, https://doi.org/10.1175/1520-0493(2000)129<4071:LCCODC>2.0.CO;2, 2000.

Gao, J., Masson-Delmotte, V., Risi, C., He, Y., and Yao, T.: What controls precipitation $\delta^{18}O$ in the southern Tibetan Plateau at seasonal and intra-seasonal scales? A case study at Lhasa and Nyalam, Tellus B, 65, 21043, https://doi.org/10.3402/tellusb.v65i0.21043, 2013.

Gao, Y., Li, X., Leung, L. R., Chen, D., and Xu, J.: Aridity changes in the Tibetan Plateau in a warming climate, Environ. Res. Lett., 9, 104013, https://doi.org/10.1088/1748-9326/10/3/034013, 2014.

Gat, J.: Oxygen and hydrogen isotopes in the hydrologic cycle, Annu. Rev. Earth Pl. Sci., 24, 225-262, https://doi.org/10.1146/ANNUREV.EARTH.24.1.225, 1996.

Gedzelman, S., Lawrence, J., Gamache, J., Black, M., Hindman, E., Black, R., Dunion, J., Willoughby, H., and Zhang, X.: Probing hurricanes with stable isotopes of rain and water vapor, Mon. Weather Rev., 131, 1112-1127, https://doi.org/10.1175/1520-0493(2003)131<1112:Phwsio>2.0.Co;2, 2003.

Goff, J.A., and Gratch, S.: Low-pressure properties of water from -160°F to 212 °F. Transactions of the American Society of Heating and Ventilating Engineers, 52, 95-122, 1946.

Goswami, B.N., Venugopal, V., Sengupta, D., Madhusoodanan, M.S., and Xavier, P.K.: Increasing Trend of Extreme Rain Events Over India in a Warming Environment, Science, 314, 1442-1445, https://doi.org/10.1126/science.1132027, 2006.

Graf, P., Wernli, H., Pfahl, S., and Sodemann, H.: A new interpretative framework for below-cloud effects on stable water isotopes in vapour and rain, Atmos. Chem. Phys., 19, 747-765, https://doi.org/10.5194/acp-19-747-2019, 2019.

Guo, X., Tian, L., Wen, R., Yu, W., and Qu, D.: Controls of precipitation $\delta^{18}O$ on the northwestern Tibetan Plateau: A case study at Ngari station, Atmos. Res., 189, 141-151, https://doi.org/10.1016/j.atmosres.2017.02.004, 2017.

Hersbach, H., Bell, B., Berrisford, P., Hirahara, S., Horányi, A., Muñoz Sabater, J., Nicolas, J., Peubey, C., Radu, R., Schepers, D., Simmons, A., Soci, C., Abdalla, S., Abellan, X., Balsamo, G., Bechtold, P., Biavati, G., Bidlot, J., Bonavita, M., and Thépaut, J.N.: The ERA5 global reanalysis, Q. J. Roy. Meteor. Soc., https://doi.org/10.1002/qj.3803, 2020.

Hsu, Y-K., Holsen, T.M., and Hopke, P.K.: Comparison of hybrid receptor models to locate PCB sources in Chicago, Atmos. Environ., 37, 545-562, https://doi.org/10.1016/S1352-2310(02)00886-5, 2003.

Jayasena, H.A.H., Chandrajith, R., and Dissanayake, C.B.: Spatial variation of isotope composition in precipitation in a tropical environment: a case study from the Deduru Oya river basin, Sri Lanka, Hydrol. Process., 22, 4565-4570, https://doi.org/10.1002/hyp.7060, 2008.

Kaushal, N., Breitenbach, S.F.M., Lechleitner, F.A., Sinha, A., Tewari, V.C., Ahmad, S.M., Berkelhammer, M., Band, S., Yadava, M., Ramesh, R., and Henderson, G.M.: The Indian Summer Monsoon from a Speleothem δ^{18}O Perspective-A Review, Quaternary, 1, 29, https://doi.org/10.3390/quat1030029, 2018.

Kostrova, S.S., Meyer, H., Fernandoy, F., Werner, M., and Tarasov, P.E.: Moisture origin and stable isotope characteristics of precipitation in southeast Siberia, Hydrol. Process., 34, 51-67, https://doi.org/10.1002/hyp.13571, 2020.

Kurita, N.: Origin of Arctic water vapor during the ice-growth season, Geophys. Res. Lett., 38, https://doi.org/10.1029/2010GL046064, 2011.

Kurita, N.: Water isotopic variability in response to mesoscale convective system over the tropical ocean, J. Geophys. Res. Atmos., 118, 10,376-10,390, https://doi.org/10.1002/jgrd.50754, 2013.

Lekshmy, P.R., Midhun, M., and Ramesh, R.: Influence of stratiform clouds on δD and δ^{18}O of monsoon water vapour and rain at two tropical coastal stations, J. Hydrol, 563, 354-362, https://doi.org/10.1016/j.jhydrol.2018.06.001, 2018.

Lekshmy, P.R., Midhun, M., and Ramesh, R.: Role of moisture transport from Western Pacific region on water vapor isotopes over the Bay of Bengal, Atmos. Res., 265, 105895, https://doi.org/10.1016/j.atmosres.2021.105895, 2022.

Lekshmy, P.R., Midhun, M., Ramesh, R., and Jani, R.A.: ^{18}O depletion in monsoon rain relates to large scale organized convection rather than the amount of rainfall, Sci. Rep., 4, 5661, https://doi.org/10.1038/srep05661, 2014.

Li, L., and Garzione, C.N.: Spatial distribution and controlling factors of stable isotopes in meteoric waters on the Tibetan Plateau: Implications for paleoelevation reconstruction, Earth Planet. Sci. Lett., 460, 302-314, https://doi.org/10.1016/j.epsl.2016.11.046, 2017.

Liu, J., Ding, M., and Xiao, C.: Review on atmospheric water vapor isotopic observation and research: theory, method and modeling, Prog. Geog., 34, 340-353, https://doi.org/10.11820/dlkxjz.2015.03.009, 2015.

Liu, X., and Chen, B.: Climatic warming in the Tibetan Plateau during recent decades, Int. J. Climatol., 20, 1729-1742, https://doi.org/10.1002/1097-0088(20001130)20:14<1729::AID-JOC556>3.0.CO;2-Y, 2000.

Majoube, M.: Fractionnement en oxygène 18 entre la glace et la vapeur d'eau, Journal De Chimie Physique, 68, 625-636, 1971a.

Majoube, M.: Fractionnement en oxygène 18 et en deutérium entre l'eau et sa vapeur, Journal de Chimie Physique et de Physico Chimie Biologique, 68, 1423-1436, https://doi.org/10.1051/jcp/1971681423, 1971b.

Malmgren, B.A., Hulugalla, R., Hayashi, Y., and Mikami, T.: Precipitation trends in Sri Lanka since the 1870s and relationships to El Niño-southern oscillation, Int. J. Climatol., 23, 1235-1252, https://doi.org/10.1002/joc.921, 2003.

Masunaga, H., and Kummerow, C.: Observations of tropical precipitating clouds ranging from shallow to deep convective systems, Geophys. Res. Lett., 33, 805, https://doi.org/10.1029/2006GL026547, 2006.

Merlivat, L., and Jouzel, J.: Global climatic interpretation of the deuterium-oxygen 18 relationship for precipitation, J. Geophys. Res. Oceans., 84, 5029-5033.

https://doi.org/10.1029/JC084iC08p05029, 1979.

Midhun, M., Lekshmy, P.R., and Ramesh, R.: Hydrogen and oxygen isotopic compositions of water vapor over the Bay of Bengal during monsoon, Geophys. Res. Lett., 40, 6324-6328, https://doi.org/10.1002/2013GL058181, 2013.

Ohring, G., Gruber, A., and Ellingson, R.: Satellite Determinations of the Relationship between Total Longwave Radiation Flux and Infrared Window Radiance, J. Appl. Meteorol. Clim., 23, 416-425, https://doi.org/10.1175/1520-0450(1984)023<0416:SDOTRB>2.0.CO;2, 1984.

Pang, Z., Kong, Y., Froehlich, K., Huang, T., Yuan, L., Li, Z., and Wang, F.: Processes affecting isotopes in precipitation of an arid region, Tellus B, 63, 352-359, https://doi.org/10.1111/j.1600-0889.2011.00532.x, 2011.

Permana, D.S., Thompson, L.G., and Setyadi, G.: Tropical West Pacific moisture dynamics and climate controls on rainfall isotopic ratios in southern Papua, Indonesia, J. Geophys. Res. Atmos., 121, 2222-2245, https://doi.org/10.1002/2015JD023893, 2016.

Pfahl, S., and Wernli, H.: Lagrangian simulations of stable isotopes in water vapor: An evaluation of nonequilibrium fractionation in the Craig-Gordon model, J. Geophys. Res. Atmos., 114, 108, https://doi.org/10.1029/2009JD012054, 2009.

Rahul, P., Ghosh, P., and Bhattacharya, S.K.: Rainouts over the Arabian Sea and Western Ghats during moisture advection and recycling explain the isotopic composition of Bangalore summer rains, J. Geophys. Res. Atmos., 121, 6148-6163, https://doi.org/10.1002/2015JD024579, 2016a.

Rahul, P., Ghosh, P., Bhattacharya, S.K., and Yoshimura, K.: Controlling factors of rainwater and water vapor isotopes at Bangalore, India: Constraints from observations in 2013 Indian monsoon, J. Geophys. Res. Atmos., 121, 13,936-13,952, https://doi.org/10.1002/2016JD025352, 2016b.

Ranjan, S., Al, R., Keesari, T., Singh, V., Kumar, P., and Manish Leuenberger, M.: Triple Water Vapour-Isotopologues Record from Chhota Shigri, Western Himalaya, India: A Unified Interpretation based on $\delta^{17}O$, $\delta^{18}O$, δD and Comparison to

Meteorological Parameters, Front. Earth Sci., 8, 599-632, https://doi.org/10.3389/feart.2020.599632, 2021.

Ravisankar, L., Madhavan, M., and Ramesh, R.: Spatial variation of amount effect over peninsular India and Sri Lanka: Role of seasonality, Geophys. Res. Lett., 42, 5500-5507, https://doi.org/10.1002/2015GL064517, 2015.

Risi, C., Bony, S., and Vimeux, F.: Influence of convective processes on the isotopic composition (δ^{18}O and δD) of precipitation and water vapor in the tropics: 2. Physical interpretation of the amount effect, J. Geophys. Res. Atmos., 113, 306, https://doi.org/10.1029/2008JD009943, 2008.

Salamalikis, V., Argiriou, A.A., and Dotsika, E.: Stable isotopic composition of atmospheric water vapor in Patras, Greece: A concentration weighted trajectory approach, Atmos. Res., 152, 93-104, https://doi.org/10.1016/j.atmosres.2014.02.021, 2015.

Saranya, P., Krishan, G., Rao, M.S., Kumar, S., and Kumar, B.: Controls on water vapor isotopes over Roorkee, India: Impact of convective activities and depression systems, J. Hydrol., 557, 679-687, https://doi.org/10.1016/j.jhydrol.2017.12.061, 2018.

Schumacher, C.: Shallow tropical convection: How often does it rain? Bull. Am. Meteorol. Soc., 87, 23-25, 2006.

Singh, P., and Bengtsson, L.: Hydrological sensitivity of a large Himalayan basin to climate change, Hydrol. Process., 18, 2363-2385, https://doi.org/10.1002/hyp.1468, 2004.

Srivastava, R., Ramesh, R., Gandhi, N., Jani, R.A., and Singh, A.K.: Monsoon onset signal in the stable oxygen and hydrogen isotope ratios of monsoon vapor, Atmos. Environ., 108, 117-124, https://doi.org/10.1016/j.atmosenv.2015.02.062, 2015.

Steen-Larsen, H.C., Masson-Delmotte, V., Hirabayashi, M., Winkler, R., Satow, K., Prié, F., Bayou, N., Brun, E., Cuffey, K., Dahl-Jensen, D., Dumont, M., Guillevic, M., Kipfstuhl, J., Landais, A., Popp, T., Risi, C., Steffen, K., Stenni, B., and Sveinbjörnsdottir, A.: What controls the isotopic composition of Greenland surface snow? Clim. Past., 10, 379-392, https://doi.org/10.5194/cpd-9-6035-2013, 2013a.

Steen-Larsen, H.C., Johnsen, S.J., Masson-Delmotte, V., Stenni, B., Risi, C., Sodemann, H., Balslev-Clausen, D., Blunier, T., Dahl-Jensen, D., Ellehøj, M.D., Falourd, S., Grindsted, A., Gkinis, V., Jouzel, J., Popp, T., Sheldon, S., Simonsen, S.B., Sjolte, J., Steffensen, J.P., Sperlich, P., Sveinbjörnsdóttir, A.E., Vinther, B.M., and White, J.W.C.: Continuous monitoring of summer surface water vapor isotopic composition above the Greenland Ice Sheet, Atmos. Chem. Phys., 13, 4815-4828, https://doi.org/10.5194/acp-13-4815-2013, 2013b.

Steen-Larsen, H.C., Sveinbjörnsdottir, A.E., Jonsson, T., Ritter, F., Bonne, J-L., Masson-Delmotte, V., Sodemann, H., Blunier, T., Dahl-Jensen, D., and Vinther, B.M.: Moisture sources and synoptic to seasonal variability of North Atlantic water vapor isotopic composition, J. Geophys. Res. Atmos., 120, 5757-5774, https://doi.org/10.1002/2015JD023234, 2015.

Stewart, M.K.: Stable isotope fractionation due to evaporation and isotopic exchange of falling waterdrops: Applications to atmospheric processes and evaporation of lakes, J. Geophys. Res., 80, 1133-1146, https://doi.org/10.1029/JC080i009p01133, 1975.

Sturm, P., and Knohl, A.: Water vapor δ^2H and δ^{18}O measurements using off-axis integrated cavity output spectroscopy, Atmos. Meas. Tech., 3, 67-77, https://doi.org/10.5194/amt-3-67-2010, 2010.

Thompson, L.G., Davis, M.E., Mosley-Thompson, E., Beaudon, E., Porter, S.E., Kutuzov, S., Lin, P.N., Mikhalenko, V.N., and Mountain, K.R.: Impacts of Recent Warming and the 2015/2016 El Niño on Tropical Peruvian Ice Fields, J. Geophys. Res. Atmos., 122, 12,688-12,701, https://doi.org/10.1002/2017JD026592, 2017.

Tremoy, G., Vimeux, F., Mayaki, S., Souley, I., Cattani, O., Risi, C., Favreau, G., and Oi, M.: A 1-year long δ^{18}O record of water vapor in Niamey (Niger) reveals insightful atmospheric processes at different timescales, Geophys. Res. Lett., 39(8), 805, https://doi.org/10.1029/2012GL051298, 2012.

Uemura, R., Matsui, Y., Yoshimura, K., Motoyam, H., and Yoshida, N.: Evidence of deuterium excess in water vapor as an indicator of ocean surface conditions, J. Geophys. Res. Atmos., 113, D19114, https://doi.org/10.1029/2008JD010209, 2008.

Villiger, L., and Aemisegger, F.: Water isotopic characterisation of the cloud–circulation coupling in the North Atlantic trades – Part 2: The imprint of the atmospheric circulation at different scales, Atmos. Chem. Phys., 24, 957-976, https://doi.org/10.5194/acp-24-957-2024, 2024.

Vimeux, F., Tremoy, G., Risi, C., and Gallaire, R.: A strong control of the South American SeeSaw on the intra-seasonal variability of the isotopic composition of precipitation in the Bolivian Andes, Earth. Planet. Sci. Lett., 307, 47-58, https://doi.org/10.1016/j.epsl.2011.04.031, 2011.

Wallace, J.M., and Hobbs, P.V.: 3-Atmospheric Thermodynamics, Atmos. Sci., 63-111, https://doi.org/10.1016/B978-0-12-732951-2.50008-9, 2006.

Wang, B.: The Asian monsoon. Springer praxis books, Springer/Praxis Publishing Co, Berlin, 787 pp., 651-683, 2006.

Webster, P.J., Magana, V.O., Palmer, T.N., Shukla, J., Tomas, R.A., Yanai, M., and Yasunari, T.: Monsoons: Processes, predictability, and the prospects for prediction, J. Geophys. Res. Oceans., 103, 14451-14510, https://doi.org/10.1029/97JC02719, 1998.

Worden, J., Noone, D., Bowman, K., Beer, R., Eldering, A., Fisher, B., Gunson, M., Goldman, A., Herman, R., Kulawik, S., Lampel, M., Osterman, G., Rinsland, C., Rodgers, C., Sander, S., Shephard, M., Webster, C., and Worden, H.: Importance of rain evaporation and continental convection in the tropical water cycle, Nature, 445, 528-532, https://doi.org/10.1038/nature05508, 2007. Xu, T., Pang, H., Zhan, Z., Zhang, W., Guo, H., Wu, S., and Hou, S.: Water vapor isotopes indicating rapid shift among multiple moisture sources for the 2018-

2019 winter extreme precipitation events in southeastern China, Hydrol. Earth Syst. Sci., 26, 117-127, https://doi.org/10.5194/hess-26-117-2022, 2022.

Yao, T., Thompson, L.G., Mosbrugger, V., Zhang, F., Ma, Y., Luo, T., Xu, B., Yang, X., Joswiak, D.R., Wang, W., Joswiak, M.E., Devkota, L.P., Tayal, S., Jilani, R., and Chen, F.: Third Pole Environment (TPE), Environ. Dev., 7, 52-64, https://doi.org/10.1016/j.envdev.2012.04.002, 2012.